4. Fauve, S. & Heslot, F. *Phys. Lett.* A**97,** 5–7 (1983).
5. Moss, F., Pierson, D. & O'Gorman, D. *Int. J. Bifurc. Chaos* **4,** 1383–1397 (1994).
6. Wiesenfeld, K. & Moss, F. *Nature* **373,** 33–36 (1995).
7. Jung, P. *Phys. Rep.* **234,** 175–295 (1993).
8. Hibbs, A. D. *et al. J. appl. Phys.* **77,** 2582–2590 (1995).
9. Longtin, A., Bulsara, A. & Moss, F. *Phys. Rev. Lett.* **67,** 656–659 (1991).
10. Bulsara, A., Jacobs, E. W., Zhou, T., Moss, F. & Kiss, L. *J. theor. Biol.* **152,** 531–555 (1991).
11. Douglass, J. K., Wilkens, L., Pantazelou, E. & Moss, F. *Nature* **365,** 337–340 (1993).
12. Moss, F., Douglass, J. K., Wilkens, L., Pierson, D. & Pantazelou, E. *Ann. N.Y. Acad. Sci.* **706,** 26–41 (1993).
13. Longtin, A. *J. statist. Phys.* **70,** 309–327 (1993).
14. Chialvo, D. R. & Apkarian, A. V. *J. statist. Phys.* **70,** 375–391 (1993).
15. Wiesenfeld, K., Pierson, D., Pantazelou, E., Dames, C. & Moss, F. *Phys. Rev. Lett.* **72,** 2125–2129 (1994).
16. Denk, W. & Webb, W. W. *Phys. Rev. Lett.* **63,** 207–210 (1989).
17. Croner, L. J., Purpura, K. & Kaplan, E. *Proc. natn. Acad. Sci. U.S.A.* **90,** 8128–8130 (1993).
18. Braun, H. A., Wissing, H., Schäfer, K. & Hirsch, M. C. *Nature* **367,** 270–273 (1994).
19. Shepherd, G. M. *Neurobiology*, 2nd edn (Oxford Univ. Press, 1988).
20. Pantazelou, E., Moss, F. & Chialvo, D. in *Noise in Physical Systems and 1/f Fluctuations* (eds Handel, P. H. & Chung, A. L.) 549–552 (Am. Inst. Physics Press, New York, 1993).
21. Knight, B. W. *J. gen. Physiol.* **59,** 734–766 (1972).
22. Collins, J. J., Chow, C. C. & Imhoff, T. T. *Phys. Rev. Lett.* (submitted).
23. Jung, P., Behn, U., Pantazelou, E. & Moss, F. *Phys Rev.* A**46,** R1709–R1712 (1992).
24. Kiss. L. B. *et al. J. statist. Phys.* **70,** 451–462 (1993).
25. Bulsara, A. R. & Schmera, G. *Phys. Rev.* E**47,** 3734–3737 (1993).
26. Neiman, A. & Schimansky-Geier, L. *Phys. Lett.* A**197,** 379–386 (1995).
27. Inchiosa, M. E. & Bulsara, A. R. *Phys. Lett.* A**200,** 283–288 (1995).
28. Inchiosa, M. E. & Bulsara, A. R. *Phys. Rev.* E (in the press).
29. Inchiosa, M. E., Bulsara, A. R., Lindner, J. F., Meadows, B. K. & Ditto, W. L. in *Proc. 3rd Technical Conf. on Nonlinear Dynamics (Chaos) and Fu!! Spectrum Processing* (Am. Inst. Physics Press, New York, in the press).
30. Lindner, J. F., Meadows, B. K., Ditto, W. L., Inchiosa, M. E. & Bulsara, A. R. *Phys. Rev. Lett.* (in the press).
31. Kiss, L. B. in *Proc. 3rd Technical Conf. on Nonlinear Dynamics (Chaos) and Full Spectrum Processing* (Am. Inst. Physics Press, New York, in the press).
32. Gingl, Z., Kiss, L. & Moss, F. *Europhys. Lett.* **29,** 191–196 (1995).
33. Kramers, H. A. *Physica* **7,** 284–302 (1940).
34. De Luca, C. J., LeFever, R. S., McCue, M. P. & Xenakis, A. P. *J. Physiol.* **329,** 113–128 (1982).
35. Mannella, R. & Palleschi, V. *Phys. Rev.* A**40,** 3381–3386 (1989).

ACKNOWLEDGEMENTS. We thank A. Pavlik for assistance with the preparation of figures. This work was supported by the US National Science Foundation.

Why gold is the noblest of all the metals

B. Hammer*† & J. K. Nørskov*

* Centre for Atomic-scale Materials Physics, Physics Department, Technical University of Denmark, DK-2800 Lyngby, Denmark
† Joint Research Center for Atom Technology (JRCAT), 1-1-4 Higashi, Tsukuba, Ibaraki 305, Japan

THE unique role that gold plays in society is to a large extent related to the fact that it is the most noble of all metals: it is the least reactive metal towards atoms or molecules at the interface with a gas or a liquid. The inertness of gold does not reflect a general inability to form chemical bonds, however—gold forms very stable alloys with many other metals. To understand the nobleness of gold, we have studied a simple surface reaction, the dissociation of H_2 on the surface of gold and of three other metals (copper, nickel and platinum) that lie close to it in the periodic table. We present self-consistent density-functional calculations of the activation barriers and chemisorption energies which clearly illustrate that nobleness is related to two factors: the degree of filling of the antibonding states on adsorption, and the degree of orbital overlap with the adsorbate. These two factors, which determine both the strength of the adsorbate–metal interaction and the energy barrier for dissociation, operate together to the maximal detriment of adsorbate binding and subsequent reactivity on gold.

In discussing nobleness, we distinguish between the ability of the metal to form and break bonds at the surface, and its ability to form new compounds (such as oxides and carbides) or be dissolved. The latter ability is closely related to the former: to form a compound it is necessary that the metal is able to bond to other atoms, but the formation of a new compound or the dissolution of the metal also involves the breaking of the metal–metal bonds. We first consider the surface reactivity of the metals and then comment on the consequences for the more general 'bulk-nobleness'.

Figure 1 summarizes the calculated reaction energetics for H_2 on the (111) surface of the four metals, Ni, Cu, Pt and Au. It can be seen that H_2 dissociation is activated on Cu and Au, and non-activated on Ni and Pt, in complete agreement with experimental evidence[1,8] and previous calculations where available (Ni, Cu)[9–13]. It is also seen that Au stands out as having both the highest barrier for dissociation and the least stable chemisorption state. The lack of reactivity of gold is thus clearly borne out by the calculations.

As a starting point for analysing the repulsive hydrogen–gold interaction we consider in Fig. 2*a* the simple two-level interaction problem. When the electronic states of two atoms overlap, quantum mechanics dictates that they be orthogonal to each other. This drives up the energy and leads to so-called Pauli repulsion. However, the overlapping states will also hybridize and form bonding and antibonding states. If only the bonding state becomes occupied, the hybridization effect will be attractive and will counteract the orthogonalization energy cost. If, on the other hand, both the bonding and antibonding state become occupied no hybridization energy is gained and the orthogonalization energy cost prevails.

This simple two-level problem can be transferred to the case of hydrogen chemisorption on the transition-metal and noble-metal surfaces. Here the adsorbate–surface interaction is most conveniently considered in two steps[14–16]. First, the interaction of the hydrogen 1*s* state with the metal 4*s* (Ni and Cu) or 6*s* (Pt and Au) band leads to a deep-lying filled bonding state and an empty antibonding state. This interaction is therefore attractive and, as the *s*–*s* coupling matrix element varies little for the metals considered, the attraction should be about the same for all four surfaces[17,18]. Then follows the interaction of the bonding state with the metal *d* states. As illustrated in Fig. 2*b* this results in an extra bonding shift of the hydrogen-induced state, but also

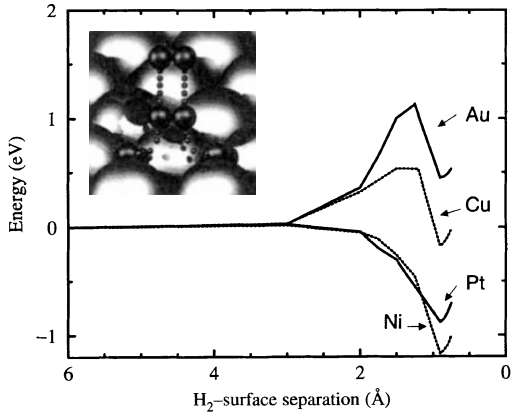

FIG. 1 Main figure, the calculated energy along the minimum-energy reaction path for H_2 dissociating on the (111) surface of Ni, Cu, Pt and Au. The H_2–surface separation is the height of the molecular centre of mass above the plane of the surface atoms. For each height, the H–H bond length has been allowed to relax to give the lowest-energy configuration, and in a similar way the configuration of the molecule relative to the surface unit cell has been allowed to relax on the way towards the surface. Inset, the calculated reaction path for H_2 dissociating on the Au(111) surface. The reaction paths on the other metals also involve an orientation of the molecular axis parallel to the surface. The calculations are done for a super-cell geometry with one H_2 molecule per $\sqrt{3} \times \sqrt{3}$ surface unit cell on one side of metal slabs consisting of four atomic (111) layers. The total energies are calculated from density-functional theory[20] describing exchange and correlation effects in the local density approximation augmented by non-local corrections in the so-called generalized gradient approximation (GGA)[21].

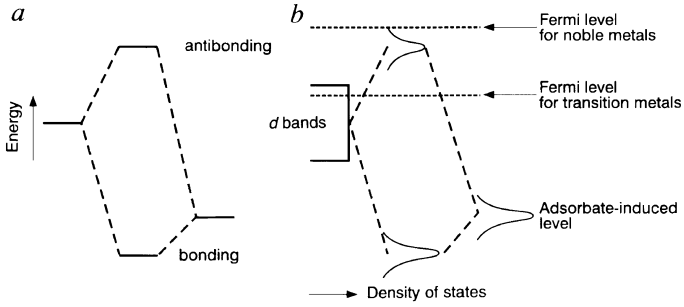

FIG. 2 Schematic illustration of the interaction between two electronic states. The down-shift of the bonding state is smaller than the up-shift of the antibonding state because the overlap of the initial states gives rise to an energy cost related to the orthogonalization of the two states. Both the energy associated with the orthogonalization, and the hybridization energy associated with the formation of bonding and antibonding states, scale with the square of the coupling matrix element. *a*, The simple case of two sharp atomic or molecular states. *b*, The interaction between a state of an adsorbate outside a metal surface, which has been broadened out to a resonance owing to the interaction with the metal *s* band, and the metal *d* bands.

in an antibonding state right above the metal *d* bands. The energy associated with this hybridization interaction must depend on the filling of the antibonding state and the coupling matrix elements V_{sd} between the *s* state and the *d* states, and we suggest that it is this contribution to the bonding which determines all the trends in the atomic chemisorption energies seen in Fig. 1.

To see this, we consider now the self consistently calculated density of one-electron states (DOS) of chemisorbed hydrogen on the four surfaces (Fig. 3). The results of the full calculations are seen to resemble the simple picture of Fig. 2*b* very well. In particular, as indicated by the upper four arrows in Fig. 3, the antibonding states just above the *d* bands are clearly seen. Although these antibonding states are empty on Ni and Pt, they are essentially filled on Cu and Au. On Ni and Pt, the coupling to the metal *d* bands therefore gives rise to an extra attraction on top of the contribution attributable to the interaction with the metal *s* band, but gives rise to a repulsion for the noble metals Cu and Au (ref. 13). Still, however, the bond between the hydrogen atom and the noble metals is not weak—the coupling to the metal *s* band gives rise to a sizeable attraction which is only partly compensated for by the repulsive interaction with the *d* bands—but relative to the bonding in the H_2 molecule, the bond is only marginally stable for Cu and completely unstable for Au.

To see why Au is more noble than Cu, we have to consider the absolute magnitude of the coupling matrix element V_{sd} (and the overlap S_{sd} which is essentially proportional to V_{sd}). The orthogonalization energy between adsorbate and metal *d* states increases monotonically with V_{sd}^2, which is considerably larger for the 5*d* metals than the 3*d* metals because of the more extended 5*d* states[17,18]. The orthogonalization energy cost therefore increases down through the groups of the periodic table rendering Au less reactive than Cu.

The concepts emerging from the above H_2-on-metal calculations now enables a more general discussion of surface nobleness. The important factors are: (1) the degree of filling of the antibonding adsorbate–metal *d* states, and (2) the size of the coupling matrix element. The filling increases to the right in the transition-metal series, and is complete for the noble metals (Cu, Ag and Au); the size of the coupling matrix element increases down through the groups of the periodic table, making the 5*d* metals the most noble. The coupling matrix element also decreases to the right in the periodic table because the *d* states become more tightly bound as the nuclear charge increases. This is shown in Fig. 4. Although the net result of the two factors does not make Pt very noble in terms of its surface reactivity (hence its use as a catalyst), the net result for Au—which has both a filled antibonding adsorbate–metal *d* state and the largest coupling matrix element—is to make it the most noble metal.

The physical picture presented here for the chemisorbed state also holds for the energy barrier for dissociation. For H_2 at the transition state, the filled molecular bonding σ_g state behaves much the same as the filled H 1*s* state considered above[9,13]. The molecular antibonding σ_u^* state, however, also interacts covalently with the metal *d* states, and the strength of this interaction completely dominates the trends in the H_2 dissociation barriers over a broad range of transition-metal, noble-metal and alloy surfaces[15,19].

The physical picture for the hydrogen/metal-surface interaction is not restricted to hydrogen. Any atom or molecule with a filled one-electron level below the *d* bands will give rise to a repulsive coupling to the *d* states for the noble metals as long as the coupling matrix element is not strong enough as to push the antibonding peak above the Fermi level (compare Fig. 2). Such low-lying states (after the interaction with the metal *s* band has been taken into account) are typical of all the simple gas atoms such as H, C, N and O (ref. 16).

We now turn to the more general nobleness—the ability of the metal to form stable compounds (such as hydrides, oxides and carbides) or to be dissolved. Again the ability to form stable bonds with H, C, N, O and so on must be governed by the processes discussed above. The noble metals, and gold in particular will form the weakest bonds. When a new compound is formed the metal–metal bonds are broken, and this introduces a third factor determining the 'bulk-nobleness', namely the cohesive energy of the metal. This is also included in Fig. 4. It is seen how the 5*d* metals have the largest cohesive energies and they therefore appear more noble in this regard. This in particular explains why Pt is usually considered more noble than Cu despite the fact that Cu surfaces are less reactive than Pt surfaces[1,5,7].

In the picture developed above, the nobleness of gold is related to the size of the overlap between the interacting atoms or molecule and the gold *d* states. Clearly, the longer the bond, the smaller the overlap and the less noble gold will appear. This

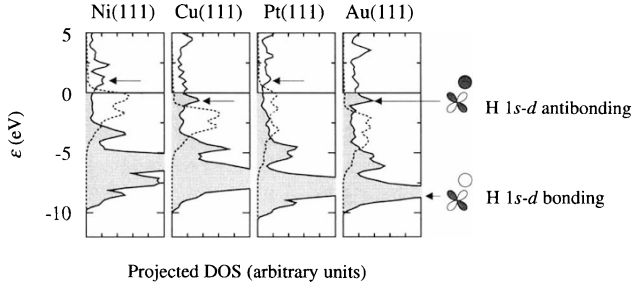

FIG. 3 The density of one-electron states (DOS) (solid lines) for H atomically chemisorbed on the (111) surface of Ni, Cu, Pt and Au. The DOS is projected onto the atomic H 1*s* state. The surface *d* bands DOS (dashed lines) of the four clean metal surfaces are shown for comparison. The dominant features are the H 1*s*–metal *d* bonding resonances at energies, ε, between −5 and −10 eV. Also prominent are the H 1*s*-metal *d* antibonding DOS peaks (indicated by arrows) directly above the metal *d* bands. These antibonding states cause repulsion on Cu and Au, where they are filled. As indicated by the grey-shading, only states below the Fermi energy (which is the energy zero in all cases) are filled.

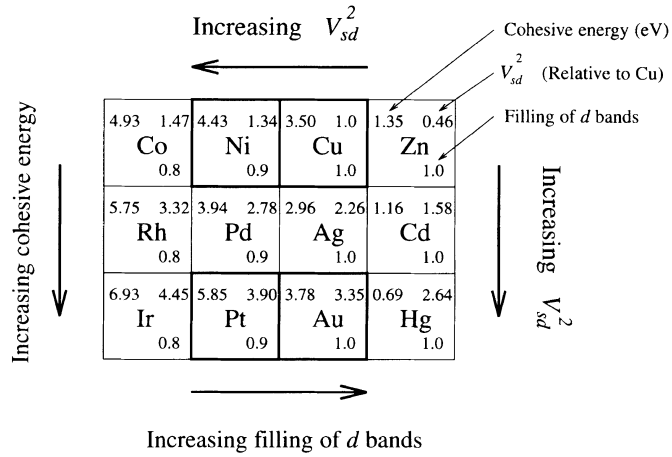

FIG. 4 The *s–d* coupling matrix element (V_{sd}^2; refs 17, 18), the filling of the metal *d* bands and the cohesive energy[22] for metals in the vicinity of gold in the periodic table. The filling of the metal *d* bands is taken as a measure of the filling of the adsorbate–metal *d* antibonding state. The largest adsorbate–metal *d* repulsion, and hence the largest nobleness in terms of the surface reactivity, is obtained by maximizing V_{sd}^2 and having an antibonding state filling of one. This is obtained for gold. The nobleness in terms of ability to resist corrosion and dissolution further involves the cohesive energy of the metals. This energy is largest for the 5*d* metals like Ir and Pt and adds particularly to the nobleness of these metals.

explains why gold is able to form metallic alloys, because the bond lengths here are very long. □

Received 24 February; accepted 27 June 1995.

1. Hayden, B. E. & Lamont, C. L. A. *Phys. Rev. Lett.* **63,** 1823–1825 (1989).
2. Hodgson, A., Moryl, J., Traversaro, P. & Zhao, H. *Nature* **356,** 501–504 (1992).
3. Michelsen, H. A., Rettner, C. T. & Auerbach, D. J. *Phys. Rev. Lett.* **69,** 2678–2681 (1992).
4. Michelsen, H. A., Rettner, C. T., Auerbach, D. J. & Zare, R. N. *J. chem. Phys.* **98,** 8294–8307 (1993).
5. Berger, H. F., Leisch, M., Winkler, A. & Rendulic, K. D. *Chem. Phys. Lett.* **175,** 425–428 (1990).
6. Robota, H. J., Vielhaber, W., Lin, M. C., Segner, J. & Ertl, G. *Surf. Sci.* **155,** 101–120 (1985).
7. Brown, J. K., Luntz, A. & Schultz, P. A. *J. chem. Phys.* **95,** 3767–3774 (1991).
8. Jaffey, D. M. & Madix, R. J. *Surf. Sci.* **311,** 159–171 (1994).
9. Hammer, B., Scheffler, M., Jacobsen, K. W. & Nørskov, J. K. *Phys. Rev. Lett.* **73,** 1400–1403 (1994).
10. White, J. A., Bird, D. M., Payne, M. C. & Stich, I. *Phys. Rev. Lett.* **73,** 1404–1407 (1994).
11. Gross, A., Hammer, B., Scheffler, M. & Brenig, W. *Phys. Rev. Lett.* **73,** 3121–3124 (1994).
12. Feibelman, P. J. & Harris, J. *Nature* **372,** 135–136 (1994).
13. Hammer, B. & Scheffler, M. *Phys. Rev. Lett.* **74,** 3487–3490 (1995).
14. Lundqvist, B. I., Gunnarsson, O., Hjelmberg, H. & Nørskov, J. K. *Surf. Sci.* **89,** 196–225 (1979).
15. Holloway, S., Lundqvist, B. I. & Nørskov, J. K. in *Proc. int. Congr. on Catalysis* 85–95 (Chemie, Berlin, 1984).
16. Nørskov, J. K. *Rep. Prog. Phys.* **53,** 1253–1295 (1990).
17. Andersen, O. K., Jepsen, O. & Glötzel, D. *Highlights of Condensed Matter Theory* Vol. LXXXIX 59 (Corso Soc. Italiana di Fisica, Bologna, 1985).
18. Nørskov, J. K. *J. chem. Phys.* **90,** 7461–7471 (1989).
19. Hammer, B. & Nørskov, J. K. *Surf. Sci.* (submitted).
20. Payne, M. C., Teter, M. P., Allan, D. C., Arias, T. A. & Joannopoulos, J. D. *Rev. mod. Phys.* **64,** 1045–1097 (1992).
21. Perdew, J. P. *et al. Phys. Rev.* B**46,** 6671–6687 (1992).
22. Kittel, C. *Introduction to Solid State Physics* (Wiley, New York, 1968).

ACKNOWLEDGEMENTS. We thank B. I. Lundqvist, I. Chorkendorff, E. Törnqvist and A. Ruban for valuable input to this work. These calculations were performed on the JRCAT supercomputing system, which is supported by the New Energy and Industrial Technology Development Organization (NEDO) of Japan. The present work was in part supported by The Centre for Surface Reactivity which is sponsored by the Danish Research Councils; the Centre for Atomic-scale Materials Physics is sponsored by the Danish National Research Foundation.

Latitudinal gradient of atmospheric CO_2 due to seasonal exchange with land biota

A. Scott Denning*, Inez Y. Fung† & David Randall*

* Department of Atmospheric Science, Colorado State University, Fort Collins, Colorado 80521, USA
† National Aeronautics and Space Administration, Goddard Space Flight Center, Institute for Space Studies, 2880 Broadway, New York, New York 10025, USA and School of Earth and Ocean Sciences, University of Victoria, Victoria, British Columbia V8W 2Y2, Canada

THE concentration of carbon dioxide in the atmosphere is increasing, largely because of fossil-fuel combustion, but the rate of increase is only about half of the total emission rate[1]. The balance of the carbon must be taken up in the oceans and the terrestrial biosphere, but the relative importance of each of these sinks—as well as their geographical distribution and the uptake mechanisms involved—are still a matter of debate[1–4]. Measurements of CO_2 concentrations at remote marine sites[5–9] have been used with numerical models of atmospheric transport to deduce the location, nature and magnitude of these carbon sinks[2,10–19]. One of the most important constraints on such estimates is the observed interhemispheric gradient in atmospheric CO_2 concentration. Published models that simulate the transport of trace gases suggest that the gradient is primarily due to interhemispheric differences in fossil-fuel emissions, with small contributions arising from natural exchange of CO_2 with the various carbon reservoirs. Here we use a full atmospheric general circulation model with a more realistic representation of turbulent mixing near the ground to investigate CO_2 transport. We find that the latitudinal (meridional) gradient imposed by the seasonal terrestrial biota is nearly half as strong as that imposed by fossil-fuel emissions. Such a contribution implies that the sinks of atmospheric CO_2 in the Northern Hemisphere must be stronger than previously suggested.

Many previous studies of CO_2 transport in the atmosphere used the transport model developed at the Goddard Institute for Space Studies (GISS) of the National Aeronautics and Space Administration[2,11–14,17,18], which prescribes the three-dimensional wind field at four-hour time intervals from the output of an atmospheric general circulation model (GCM). Sub-grid-scale vertical transport of trace gases is simulated in terms of prescribed monthly mean convective frequencies in the parent GCM. Interhemispheric mixing in the model is tuned using an adjustable sub-grid diffusion parameter to produce realistic meridional gradients for tracers with known aseasonal, mid-latitude sources. The annual mean meridional gradient in atmospheric CO_2 simulated by the GISS model is much stronger than observed when the effects of fossil-fuel emissions, seasonal exchange with the terrestrial biota, and emissions from tropical deforestation and from the equatorial oceans are included (about 5 or 6 parts per million by volume (p.p.m.v.) from the Arctic to the Antarctic, as compared to an observed gradient of about 3 or 4 p.p.m.v.)[2]. This implies the existence of sinks of CO_2 in the Northern Hemisphere so strong as to be inconsistent with available oceanographic data[2]. Thus at least some of the Northern Hemisphere sink is believed to be terrestrial, and is thought to be due to direct CO_2 fertilization[20], nutrient deposition[21], reforestation[22] and/or climate fluctuations[23].

Although it has long been recognized that atmospheric dispersion of pollutants released at the ground surface depends